CAAI Transactions on Intelligence Technology

Special Issue: Recent Advances in Intelligent Robotic Systems

Magnetic orientation system based on magnetometer, accelerometer and gyroscope

ISSN 2468-2322
Received on 9th September 2017
Revised on 8th November 2017
Accepted on 20th November 2017
doi: 10.1049/trit.2017.0024
www.ietdl.org

Zhiwei Chu[1,2,3], Chilai Chen[1,3], Youjiang Liu[1,3], Yingxian Wang[1,3], Xinhua Lin[1,3] ✉

[1]*State Key Laboratory of Transducer Technology, Hefei Institute of Physical Science, Chinese Academy of Sciences, Hefei 230031, People's Republic of China*
[2]*Department of Automation, School of Information Science and Technology, University of Science and Technology of China, Hefei 230026, People's Republic of China*
[3]*Key Laboratory of Biomimetic Sensing and Advanced Robot Technology of Anhui Province, Hefei Institute of Physical Science, Chinese Academy of Sciences, Hefei 230031, People's Republic of China*
✉ *E-mail: xhlin@iim.ac.cn*

Abstract: Magnetic orientation systems have widely been used by measuring the earth magnetic field and provide a pervasive source of directional information. However, to obtain the high precision, orientation systems must be compensated prior to use for the various errors of magnetometers such as the bias, misalignment and inconsistence in sensitivity, and the pitch and roll angles, especially in dynamic state. In this study, magnetic orientation system mainly consist of three single-axis magnetometers, a tri-axis accelerometer and a tri-axis gyroscope were developed. An error-separation method was introduced to calibrate magnetometers. Data from magnetometers, accelerometer and gyroscope were fused based on Kalman filtering. In addition, accelerometer and gyroscope were also calibrated before data fusion. Experimental results showed the heading error of magnetic orientation system was about 0.1° in a static state, and <3° in a dynamic state, which proved the effectivities of the calibration methods and data fusion algorithm.

1 Introduction

The magnetic azimuth is the angle relative to the orientation of the earth magnetic field component in the horizontal plane, indicating the knowledge of the horizontal or vertical plane must be required to correct the measured magnetic value in the application of magnetic orientation systems. The tilt angles are commonly obtained by measuring the gravity vector at rest. In the previous report [1], it has been shown that the azimuth derived from the values of magnetometers and tilt contains and propagates the errors present in the attitude angles themselves. Thus, the orientation precision of magnetic orientation systems not only depends on the calibration validity of magnetometers, but also was closely related to the errors of tilt angles.

Usually, accelerometers are used to compensate for the azimuth by achieving attitude angles information [2–8]. In these references, the magnetic orientation systems have high precision partly because they are working in a static state. However, when the magnetic orientation system works in the dynamical state, the acceleration field obtained from the accelerometers contains kinematic acceleration besides gravitational acceleration. Thus, the real dynamic attitude of magnetic orientation systems cannot be resolved from the output of accelerometers. As a result, just based on the data of magnetometers and accelerometers the azimuth error of magnetic orientation systems will be enlarged in the case of movement. Especially, when the kinematic acceleration disturbance is violent, the magnetic orientation systems will lose their functionality.

To deal with this problem, gyroscopes are introduced into magnetic orientation systems [9–15]. These studies mainly focus on the sensor fusion algorithms and less analysis is applied to the calibration of sensors. However, the large measurement error in the output of sensors will lead to a large error of the data fusion results and poor convergence ability. Thus, at first magnetometer, accelerator and gyroscope in magnetic orientation system must be calibrated in order to obtain the actual real-time azimuth and attitude through the data fusion algorithm. Complementary filter (CF) algorithm is widely used in the field of unmanned aerial vehicles and micro aerial vehicles. For the CF, a set of attitude angles are estimated in each measurement and they are multiplied with the corresponding gain factors. The eventual attitude angles are the sum of the parts. The more accurate estimations can be made by adjusting the gain factors. CF can be realised easily, but its accuracy is relatively low. It is only suitable for the low-dynamic application due to its slow response [16–20]. The quaternion-based extended Kalman filter (EKF) is appropriate for non-linear plant models. Among the variants of the Kalman filtering framework, EKF is the most prominent one for its relatively high accuracy. However, in this algorithm, the magnetic measurement is fused into roll and pitch, resulting in the larger error of yaw and the low precision in the pitch and roll angles once magnetic interference occurs [10, 11, 18, 20]. In addition, the Jacobi matrix needs to be calculated in EKF, which will introduce the linearisation error inevitably.

On the basis of the previous studies of the tri-axis magnetometer calibration with error-separation method [8], the tri-axis accelerometer calibration with multi-position method [5, 6] and the tri-axis gyroscope calibration through the method of three-position with six different angular velocities [9], a quaternion-based KF is proposed in this paper to fuse the data from sensors and to estimate the orientation. In the measurement model, the state vector of a quaternion is converted from the Euler angles which are resolved from the output of accelerometer and magnetometers instead of the accelerometer and magnetometers measurement vectors which are used in the traditional method of EKF [11]. So we can apply KF to the system without calculating the Jacobi matrix since the process model and the measurement model are linear, which means no linearisation error, lower cost of computation and less computational time. Better yet, when magnetic disturbances are present, their influence is only limited to the heading angle. The achievement of the high-precise magnetic orientation system which can work well under various operation conditions demonstrated that the calibration and data fusion

algorithm of multi-sensors is effective. Moreover, the magnetic orientation system is suited to the practical application since it is composed of commercial-off-the-shelf components.

2 Principle of magnetic orientation system without gyroscope

The case body frame of magnetic orientation system is denoted as the b coordinate frame and has three orthogonal axes of x_b, y_b and z_b. We define that x_l, y_l and z_l are the axes of the local horizontal frame (l). The x_l is along the direction of horizontal projection of x_b, z_l is along the downward direction and x_l, y_l and z_l obey the right-hand rule.

So, if θ denotes the pitch angle of the vehicle and φ denotes roll angle of the vehicle, the components of the earth magnetic field in the x_l and y_l directions can be calculated as follows:

$$\begin{aligned} h_x^l &= h_x^b \cos\theta + h_y^b \sin\theta \sin\varphi + h_z^b \sin\theta \cos\varphi \\ h_y^l &= h_y^b \cos\varphi - h_z^b \sin\varphi \end{aligned} \tag{1}$$

The magnetic heading ψ is obtained by the following formula:

$$\psi = \begin{cases} -\arctan(h_y^l/h_x^l), & (h_x^l > 0,\ h_y^l \le 0) \\ \pi/2, & (h_x^l = 0,\ h_y^l < 0) \\ \pi - \arctan(h_y^l/h_x^l), & (h_x^l < 0) \\ 3\pi/2, & (h_x^l = 0,\ h_y^l > 0) \\ 2\pi - \arctan(h_y^l/h_x^l), & (h_x^l > 0,\ h_y^l > 0) \end{cases} \tag{2}$$

where h_i^l ($i = x, y$ or z) is the component of Earth magnetic field on the i axes in the l frame; h_i^b is the component of Earth magnetic field on the i axes in the b frame. According to the first-order Taylor development of the azimuth computation [1], the uncertainty in azimuth becomes

$$\begin{aligned} \psi + \Delta\psi = \arctan\left(\frac{-h_y^l}{h_x^l}\right) &+ \frac{\partial(\arctan(-h_y^l/h_x^l))}{\partial h_x^l}\Delta h_y^l \\ &+ \frac{\partial(\arctan(-h_y^l/h_x^l))}{\partial h_y^l}\Delta h_x^l \end{aligned} \tag{3}$$

Simplifying (3) and taking into account that

$$H_e = H_h \begin{bmatrix} \cos\psi \\ -\sin\psi \\ \tan\delta \end{bmatrix} \tag{4}$$

where δ is the inclination of the magnetic vector and H_h is the horizontal magnetic field. The error produced can be written as

$$\Delta\psi = -\Delta\theta \tan\delta \cos\psi - \Delta\varphi \tan\delta \sin\psi \tag{5}$$

According to the above (1), (2) and (5), in order to improve the precision of the heading angle ψ, we must not only increase the measurement precision of h_i^b as possible, but also take into account how to compensate the errors of pitch angle θ and roll angle φ.

3 Calibration of sensors

The magnetic orientation system we developed comprises of three single-axis magnetometers, a tri-axis accelerometer and a tri-axis gyroscope. The calibration methods of sensors will be introduced as follows.

3.1 Calibration of three single-axis magnetometers

According to (2), the absolute magnitude of $h_i (i = x, y, z)$ is not necessary to compute the magnetic heading. In this paper, the error-separation method [8] is adopted to calibrate the magnetometers in consideration that it is convenient to evaluate the influence of different error sources and to get high precision of measurement. The output model of magnetometers can be expressed as follows:

$$\begin{aligned} \begin{bmatrix} h_x^m \\ h_y^m \\ h_z^m \end{bmatrix} = &\begin{bmatrix} k_x^m & 0 & 0 \\ 0 & k_y^m & 0 \\ 0 & 0 & k_z^m \end{bmatrix} \\ &\times \begin{bmatrix} \cos\angle x_m x_b & \cos\angle x_m y_b & \cos\angle x_m z_b \\ \cos\angle y_m x_b & \cos\angle y_m y_b & \cos\angle y_m z_b \\ \cos\angle z_m x_b & \cos\angle z_m y_b & \cos\angle z_m z_b \end{bmatrix} \begin{bmatrix} h_x^b \\ h_y^b \\ h_z^b \end{bmatrix} \\ &+ \begin{bmatrix} b_x^m \\ b_y^m \\ b_z^m \end{bmatrix} + \begin{bmatrix} n_x^m \\ n_y^m \\ n_z^m \end{bmatrix} \end{aligned} \tag{6}$$

where $h_i^m (i = x, y, z)$ is the raw output of magnetometer; $k_i^m (i = x, y, z)$ is the sensitivity of the magnetometer in the direction of i_m; $\cos\angle A_m B_b (A, B = x, y, z)$ is the cosine of the angles between the relevant axes in the measurement frame and in the body frame; $b_i^m (i = x, y, z)$ is the bias originated from the offset and magnetic interference; and $n_i^m (i = x, y, z)$ represents the noise of sensor and can be easily eliminated by averaging the measurements, and thereafter is ignored in this paper.

At the right-hand side of (6), the first diagonal matrix accounts for the different sensitivities of the magnetometers, the second 3×3 matrix represents the output influence from non-orthogonality and misalignment of the three magnetometers, and the bias is embodied in the matrix about b.

With the three-axis non-magnetic rotation platform, the parameters in (6) can be obtained, so the errors from the sensitivity inconsistency, the non-orthogonality and misalignment and the combined biases can be eliminated independently. Now, we get the output components of the earth magnetic field in the body frame as follows:

$$\begin{aligned} \begin{bmatrix} h_x^b \\ h_y^b \\ h_z^b \end{bmatrix} = &\begin{bmatrix} \cos\angle x_m x_b & \cos\angle x_m y_b & \cos\angle x_m z_b \\ \cos\angle y_m x_b & \cos\angle y_m y_b & \cos\angle y_m z_b \\ \cos\angle z_m x_b & \cos\angle z_m y_b & \cos\angle z_m z_b \end{bmatrix}^{-1} \\ &\times \begin{bmatrix} k_x^m & 0 & 0 \\ 0 & k_y^m & 0 \\ 0 & 0 & k_z^m \end{bmatrix}^{-1} \begin{bmatrix} h_x^m - b_x^m \\ h_y^m - b_y^m \\ h_z^m - b_z^m \end{bmatrix} \end{aligned} \tag{7}$$

Finally, the magnetic heading can be calculated by above (1) and (2). After the calibration of magnetometers is accomplished, the relevant parameters are also acquired. The angles between the axes in the measurement frame and the body frame are shown in Table 1. The characteristic curves of magnetometers acquired with a linear least-squares fit are shown in Fig. 1. According to the fitted curves, the parameters in the calibration matrix could be obtained.

Table 1 Angles between the axes in the measurement frame and the body frame

$\angle x_m x_b$ 0.0640°	$\angle x_m y_b$ 89.8353°	$\angle x_m z_b$ 89.4179°
$\angle y_m x_b$ 88.8302°	$\angle y_m y_b$ 1.9147°	$\angle y_m z_b$ 91.5156°
$\angle z_m x_b$ 90.8175°	$\angle z_m y_b$ 90.8175°	$\angle z_m z_b$ 3.0661°

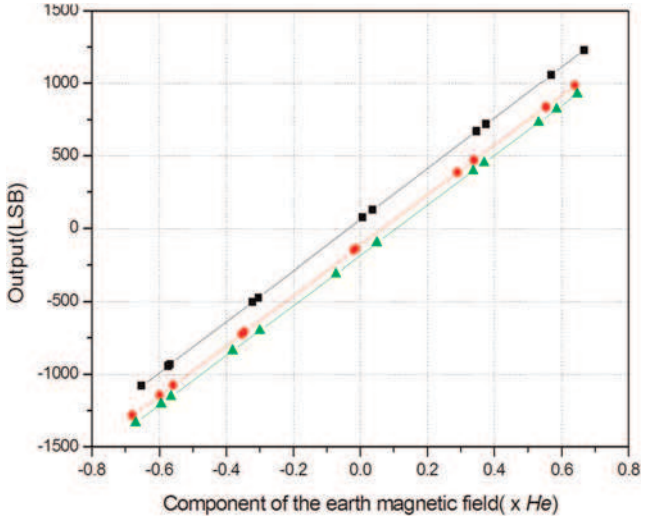

Fig. 1 *Fitted curves between the outputs of magnetometers and the component of the earth magnetic field in the direction of the magnetic sensor axes (x_m-axis: line, y_m-axis: line and z_m-axis: line) and the original outputs of magnetometers (x_m-axis: filled square, y_m-axis: filled red circle and z_m-axis: filled green triangle);* He *is equal to the magnitude of the earth magnetic field*

The result is shown as follows:

$$\begin{cases} k_x^m = 1751.15(\text{LSB}\,H_e^{-1}) \\ k_y^m = 1720.05(\text{LSB}\,H_e^{-1}) \\ k_z^m = 1717.16(\text{LSB}\,H_e^{-1}) \end{cases} \quad \begin{cases} b_x^m = 61.93(\text{LSB}) \\ b_y^m = -114.52(\text{LSB}) \\ b_z^m = -183.77(\text{LSB}) \end{cases}$$

Now all the parameters to calibrate the magnetometers have been obtained. Moreover, if the true pitch angle and roll angle (as in static state) is known, we can determine the orientation of the vehicle precisely with (1) and (2).

3.2 Calibration of tri-axis accelerometer

Unlike magnetometer, the accelerometer is immune to environmental impact because the gravity vector stays almost unchanged wherever it works. There are lots of methods to calibrate the tri-axis accelerometer. The so-called multi-position calibration is used mostly hitherto and has been proved to be effective [5, 6].

In the six-position method, the sign definition of the accelerometer raw measurements is shown in Table 2. It is worth mentioning that to compute the tilt more effectively; A_x^b is defined along the direction of x_b; and A_y^b and A_z^b are in the opposite directions of y_b and z_b, respectively. The relationship between the normalised A_i^b ($i=x$, y or z) and the raw measurement A_i ($i=x$, y or z) of the accelerometer can be expressed as the following equation:

$$\begin{bmatrix} A_x^b \\ A_y^b \\ A_z^b \end{bmatrix} = [A\_m]_{3\times3} \begin{bmatrix} 1/A\_S_x & 0 & 0 \\ 0 & 1/A\_S_y & 0 \\ 0 & 0 & 1/A\_S_z \end{bmatrix} \begin{bmatrix} A_x - A\_O_x \\ A_y - A\_O_y \\ A_z - A\_O_z \end{bmatrix} = \begin{bmatrix} A_{11} & A_{12} & A_{13} \\ A_{21} & A_{22} & A_{23} \\ A_{31} & A_{32} & A_{33} \end{bmatrix} \begin{bmatrix} A_x \\ A_y \\ A_z \end{bmatrix} + \begin{bmatrix} A_{10} \\ A_{20} \\ A_{30} \end{bmatrix} \tag{8}$$

where $[A\_m]_{3\times3}$ is the 3×3 matrix representing the misalignment between the accelerometer sensing axes and the device body axes. A_S_i ($i=x$, y or z) is the sensitivity and A_O_i ($i=x$, y or z) is the offset.

Table 2 Sign definition of the tri-axis accelerometer raw measurements

Stationary position	Accelerometer (signed integer)		
	A_x^b	A_y^b	A_z^b
Z_b down	0	0	+1 g
Z_b up	0	0	−1 g
Y_b down	0	+1 g	0
Y_b up	0	−1 g	0
X_b down	−1 g	0	0
X_b up	+1 g	0	0

Table 3 Coefficients of calibration for the tri-axis accelerometer

A_{11}	A_{12}	A_{13}	A_{10}
−0.0001773	0.0000016	0.0000016	−0.0155254
A_{21}	A_{22}	A_{23}	A_{20}
0.0000037	−0.0001800	−0.0000007	0.0227611
A_{31}	A_{32}	A_{33}	A_{30}
0.0000036	−0.0000004	0.0001801	−0.0048272

Then, the pitch and roll angles of the device can be calculated as follows:

$$\text{Pitch}(\theta) = \arctan\left(\frac{A_x^b}{\sqrt{(A_y^b)^2 + (A_z^b)^2}}\right) \tag{9}$$

$$\text{Roll}(\varphi) = \arctan\left(\frac{A_y^b}{A_z^b}\right) \tag{10}$$

According to the above formulas, the absolute magnitude of A_i^b ($i=x$, y or z) is not needed. Thus, the normalised value A_i^b ($i=x$, y or z) can be obtained from any given raw measurements at an arbitrary position as follows:

$$|A| = \sqrt{(A_x^b)^2 + (A_y^b t)^2 + (A_z^b)^2} = 1 \tag{11}$$

According to the above (8)–(10), we need 12 parameters from A_{10} to A_{33} to calibrate the tri-axis accelerometer. By mounting the magnetic orientation system on the three-dimensional (3D) rotation platform which has a high-precision digital encoder, calibration can be operated at six stationary positions as shown in Table 2. We collect at least 100 sets of data at each position and take the averages. The 12 desired coefficients are extracted from the obtained data by the least-square method as shown in Table 3.

3.3 Calibration of tri-axis gyroscope

Tri-axis gyroscope works by sensing angular velocity around the three sensitive axes. However, to ensure high precision, tri-axis gyroscope must be calibrated before use [9].

The output model of the tri-axis gyroscope can be expressed in a matrix form as follows:

$$\begin{bmatrix} G_x^b \\ G_y^b \\ G_z^b \end{bmatrix} = [G\_m]_{3\times3} \begin{bmatrix} 1/G\_S_x & 0 & 0 \\ 0 & 1/G\_S_x & 0 \\ 0 & 0 & 1/G\_S_x \end{bmatrix} \begin{bmatrix} G_x - G\_O_x \\ G_y - G\_O_y \\ G_z - G\_O_z \end{bmatrix} = \begin{bmatrix} k_{11} & k_{12} & k_{13} \\ k_{21} & k_{22} & k_{23} \\ k_{31} & k_{32} & k_{33} \end{bmatrix} \begin{bmatrix} G_x \\ G_y \\ G_z \end{bmatrix} + \begin{bmatrix} k_{10} \\ k_{20} \\ k_{30} \end{bmatrix} \tag{12}$$

where G_x, G_y and G_z are the raw measurements of the X-axis, Y-axis, and Z-axis of the gyroscope, respectively; G_x^b, G_y^b and G_z^b are the true

angular velocities around the X-axis, Y-axis, and Z-axis of the body frame; the 3×3 matrix about $[G\_m]$ accounts for misalignment between the sensitive axis and the body axis; $G\_S_i (i = x, y, z)$ is the scale factor and G_O_i is the zero bias. The calibration process is described in detail in [9]. Here, the method of three-position with six different angular velocities is adopted.

The 12 parameters about k can be calculated with the least-square method as follows:

$$K = [P^{\mathrm{T}} P]^{-1} P^{\mathrm{T}} Y \tag{13}$$

$$K = \begin{bmatrix} k_{11} & k_{21} & k_{31} \\ k_{12} & k_{22} & k_{32} \\ k_{13} & k_{23} & k_{33} \\ k_{10} & k_{20} & k_{30} \end{bmatrix} \tag{14}$$

$$P = [\, G_1 \quad G_2 \quad \ldots \quad G_{18} \,]^{\mathrm{T}} \tag{15}$$

$$Y = [\, y_1 \quad y_2 \quad \ldots \quad y_{18} \,]^{\mathrm{T}} \tag{16}$$

where $G_i (i = 1, 2, \ldots, 18)$ is a 4×1 matrix $[\, G_x \quad G_y \quad G_z \quad 1 \,]^{\mathrm{T}}$, the elements are the values gotten from the calibration process and 1. Here, $y_i (i = 1, 2, \ldots, 18)$ is a 3×1 matrix consisting of normalised output $[\, G_x^b \quad G_y^b \quad G_z^b \,]^{\mathrm{T}}$. As w_l, w_m and w_h are known [9], y_i is easy to determine.

After the processing of calibration, the matrix $\boldsymbol{K}$ is listed as follows:

$$\boldsymbol{K} = \begin{bmatrix} -0.1243681 & -0.0012937 & -0.0033316 \\ 0.0003576 & 0.1237108 & 0.0009321 \\ 0.0003312 & -0.0001178 & -0.1243840 \\ -2.3843363 & 2.3942377 & -2.1203979 \end{bmatrix} \tag{17}$$

4 Data fusion

To diminish the influence of non-gravitational acceleration, after the above calibrations, the data obtained from the sensors are further combined based on Kalman filtering with a state vector consisting of four elements (the quaternion components), a linear process model and a linear measurement model. The quaternion converted from Euler angles [computed with the (2), (9) and (10)] is taken as the measurement for the KF to correct the predicted state obtained by processing the readings provided by the angular rate sensor (the tri-axis gyroscope). Using this method, all the output equations are linear, which simplifies the design of the filter, and the non-linear error from EKF can be eliminated.

4.1 Process model

In the prediction step, the angular velocity vector, measured by the tri-axis gyroscope, is used to compute the first estimation of the orientation in quaternion form. It is well known that the rigid body angular motion obeys a vector differential equation [10, 11] describing the rate of change of the orientation as quaternion derivative

$$\frac{\mathrm{d}}{\mathrm{d}t} q = \Omega[\boldsymbol{w}] q \tag{18}$$

where

$$\Omega[\boldsymbol{w}] = \frac{1}{2} \begin{bmatrix} [\boldsymbol{w} \times] & \boldsymbol{w} \\ -\boldsymbol{w}^{\mathrm{T}} & 0 \end{bmatrix}. \tag{19}$$

$$q = \begin{bmatrix} q_1 & q_2 & q_3 & q_4 \end{bmatrix}^{\mathrm{T}} \tag{20}$$

$\boldsymbol{w}(t) = [\, w_x \quad w_y \quad w_z \,]^{\mathrm{T}}$ is the output of the tri-axis gyroscope after calibration. $\Omega[\boldsymbol{w}]$ is a 4×4 skew symmetric matrix and the operator

$$[\boldsymbol{w} \times] = \begin{bmatrix} 0 & w_z & -w_y \\ -w_z & 0 & w_x \\ w_y & -w_x & 0 \end{bmatrix} \tag{21}$$

represents the standard vector cross-product [11].

In this paper, quaternion represents the notation from

$$n = q_1 i + q_2 \mathrm{j} + q_3 k + q_4 = \boldsymbol{n} + n_0 \tag{22}$$

where q_1, q_2, q_3 and q_4 are real numbers and i, j and k are unit vectors directed along the x, y and z axes, respectively. A quaternion is unit quaternion [12] if

$$n_0 = \cos\, \theta \text{ and } |\boldsymbol{n}| = \sin\, \theta$$

The direct cosine matrix given in terms of the orientation quaternion can be expressed as the following matrix:

$$C_n^b(q) = \begin{bmatrix} q_1^2 - q_2^2 - q_3^2 + q_4^2 & 2(q_1 q_2 + q_3 q_4) & 2(q_1 q_3 - q_2 q_4) \\ 2(q_1 q_2 - q_3 q_4) & -q_1^2 + q_2^2 - q_3^2 + q_4^2 & 2(q_2 q_3 + q_1 q_4) \\ 2(q_1 q_3 + q_2 q_4) & 2(q_2 q_3 - q_1 q_4) & -q_1^2 - q_2^2 + q_3^2 + q_4^2 \end{bmatrix} \tag{23}$$

Thus, we can establish the process model such as the following equation:

$$q(k) = q(k-1) + \Omega[\boldsymbol{w}] q(k-1)\, \mathrm{d}t + \zeta(k) \tag{24}$$

where k is the sampling number and $\mathrm{d}t$ is the sampling period and

$$\zeta(k) = -\frac{\mathrm{d}t}{2} \Xi(k) v_{\mathrm{g}}(k) = -\frac{\mathrm{d}t}{2} \begin{bmatrix} -q_4 & -q_3 & -q_2 \\ q_2 & -q_4 & -q_1 \\ -q_2 & q_1 & -q_4 \\ q_1 & q_2 & q_3 \end{bmatrix} v_{\mathrm{g}}(k) \tag{25}$$

where $v_{\mathrm{g}}(k)$ is the white Gaussian measurement noise affecting the gyroscope readings, with covariance matrix $\Sigma_{\mathrm{g}} = \sigma_{\mathrm{g}}^2 I_{3\times 3}$. Finally, the process noise covariance matrix $\boldsymbol{Q}_k$ is expressed as

$$\boldsymbol{Q}_k = \left(-\frac{\mathrm{d}t}{2} \right)^2 \Xi(k) \Sigma_{\mathrm{g}} \Xi(k)^{\mathrm{T}} \tag{26}$$

4.2 Measurement model

After calibration, the Euler angles can be computed with (2), (6) and (7) according to the output of the accelerometer and the magnetometers. The quaternion converted from the Euler angles is used in the measurement update step. The transformation formula is expressed in [13]

$$Z = \begin{bmatrix} q_1 \\ q_2 \\ q_3 \\ q_4 \end{bmatrix} = \begin{bmatrix} s\varphi c\theta c\psi - c\varphi s\theta s\psi \\ c\varphi s\theta c\psi + s\varphi c\theta s\psi \\ c\varphi c\theta s\psi - s\varphi s\theta c\psi \\ c\varphi c\theta c\psi + s\varphi s\theta s\psi \end{bmatrix} \tag{27}$$

where $c\phi = \cos(\phi/2)$, $s\phi = \sin(\phi/2)$, θ is the pitch angle, φ is roll angle and ψ is the heading angle [computed with (2), (6) and (7)]. The measurement model can be expressed as the following equation:

$$Z(k) = q(k) + \xi(k) \tag{28}$$

where $\xi(k)$ is the measurement noise which is approximated as a white Gaussian noise obtained from the propagation of the

acceleration and magnetic field measurement noise [14]. The measurement noise covariance matrix is $\boldsymbol{R}_k$.

4.3 Kalman filter

As a recursive estimator, the following formulas are used in computation:

$$\begin{aligned} \boldsymbol{x}_k^- &= A\boldsymbol{x}_{k-1}^-, \\ P_k^- &= AP_{k-1}A^{\mathrm{T}} + Q_k, \\ K_k &= P_k^- H^{\mathrm{T}}(HP_k^- H^{\mathrm{T}} + R_k)^{-1}, \\ \boldsymbol{x}_k &= \boldsymbol{x}_k^- + K_k(Z_k - H\boldsymbol{x}_k^-), \\ P_k &= (I - K_k H)P_k^-, \end{aligned} \tag{29}$$

where $\boldsymbol{x}_k^-$ is the a priori estimation of the state vector; $\boldsymbol{x}_k$ is the a posteriori estimation of the state vector; $\boldsymbol{A}$ is the state matrix; $\boldsymbol{H}$ is the observation matrix; $\boldsymbol{P}$ is the error covariance matrix; $\boldsymbol{I}$ is the identity matrix; and $\boldsymbol{K}$ is the matrix of KF gain [11].

After each iteration, the magnetic orientation can be gotten from $\boldsymbol{x}_k$. As expressed in [13], the Euler angles can be computed from quaternion using the following formulas:

$$\begin{cases} \psi = (180/\pi)\, a\tan 2(2(q_4 q_3 + q_1 q_2),\ 1 - 2(q_2^2 + q_3^3)) \\ \theta = (180/\pi)\, \arcsin(2(q_4 q_2 - q_1 q_3)) \\ \varphi = (180/\pi)\, a\tan 2(2(q_4 q_1 + q_3 q_2),\ 1 - 2(q_2^2 + q_1^3)) \end{cases} \tag{30}$$

5 Experimental results

For verification of the calibration methods and the proposed algorithm of data fusion, a 3D non-magnetic platform that can rotate around three axes by the manual operation was used. Before data fusion, the accuracy of the error-separation calibration method in a static state is shown in Fig. 2, where the horizontal coordinate axis stands for platform readings. We can see that with the magnitudes of both pitch and roll angles increasing, the heading errors exhibited an increasing trend. However, the maximum error in the heading was only about 0.4° even if the magnitudes of both pitch and roll angles increased up to 60°. Moreover, precision comparisons of different calibration methods are listed in Table 4. The ellipsoid fitting method and the traditional method are provided by Fang *et al.* [5] and Yun *et al.* [7]. These results demonstrated that the calibration method of error-separation was very effective and efficient.

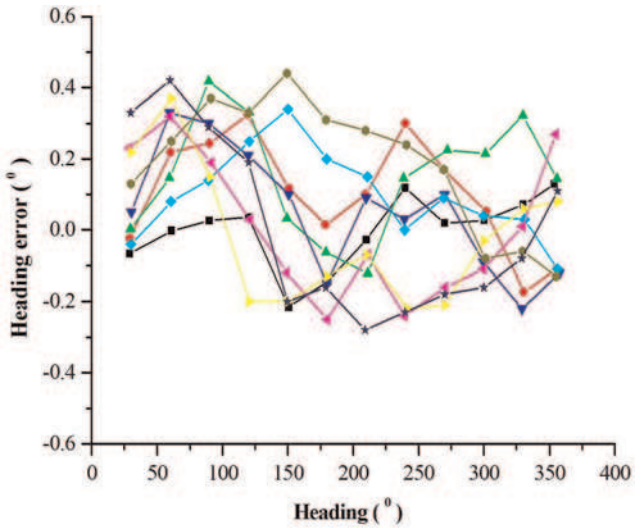

Fig. 2 *Heading errors of magnetic orientation system with the different attitudes, (filled square) $\theta = 0°$, $\gamma = 0°$; (filled dark green triangle) $\theta = 30°$, $\gamma = 30°$ and (filled inverted blue triangle) $\theta = 30°$, $\gamma = -30°$; (filled rhombus) $\theta = -30°$, $\gamma = 30°$; (left-pointed purple filled triangle) $\theta = -30°$, $\gamma = -30°$; (filled red circle) $\theta = 60°$, $\gamma = 60°$; (right-pointed yellow filled triangle) $\theta = 60°$, $\gamma = -60°$; (filled grey circle) $\theta = -60°$, $\gamma = 60°$ and (filled star) $\theta = -60°$, $\gamma = -60°$*

After calibrating the sensors, two modes of experiments had been carried out to evaluate the accuracy of our magnetic orientation system. Mode 1 is the static state and Mode 2 is the dynamic state. The results from the proposed KF (q-KF) are provided, and for comparison the corresponding results from EKF and CF are also shown.

In Mode 1, the magnetic orientation system was rigidly mounted on the 3D non-magnetic platform and was kept static (remain level: true pitch and roll angles were equal 0°) when we were collecting data outputs. The results are shown in Fig. 3. The data called Measured (blue) were computed without data fusion only from the output of the tri-axis accelerometer and the magnetometers [as (2), (9) and (10)], while the data called estimated (green) were computed by the q-KF [as (30)]. The black solid line called Reference represents the readings of the 3D non-magnetic platform. We can see that with the KF algorithm proposed in this paper, the magnetic orientation system is steadier (0.1°) than the one without data fusion (0.4°). Moreover, the errors of yaw, pitch and roll angles computed by the data fusion in our magnetic orientation system are very small as about 0.1°.

In Mode 2, the magnetic orientation system was mounted on the 3D non-magnetic platform, and then we carried out two kinds of operation conditions [Mode 2 (a) and Mode 2 (b)]. In Mode 2 (a), the roll angle was dynamically changed by manual operation when the pitch angle was kept at 0°. From Fig. 4, it can be seen that after calibration and data fusion based on q-KF (Estimated), the maximum error of yaw angle was about 2.8° and the maximum error of pitch angle was about 0.3°. However, without the data fusion (Measured), the maximum error of the yaw angle was more than 10° and the maximum error of the pitch angle was about 2.5°. In Mode 2 (b), when the roll angle was kept at 0°, the pitch angle was dynamically changed by manual operation. As shown in Fig. 5, with the q-KF the maximum errors of yaw and roll angles, decreased from about 6.5° (Measured) to about 2.5° (Estimated) and from about 2.5° (Measured) to about 1.8° (Estimated) in Mode 2 (b). The above results demonstrate that the heading and attitude precision were improved significantly with our calibration methods and data fusion algorithm based on KF. It is worth mentioning that since roll angle [Mode 2 (a)] and pitch angle [Mode 2 (b)] of the 3D non-magnetic platform was changed by manual operation, their real angle values were unobservable during changing with time. Thus, the data of roll angles [Mode 2 (a)] and pitch angles [Mode 2 (b)] are not shown in this paper.

Obviously, in the dynamic circumstance the magnetic orientation system without gyroscope and data fusion is useless and the errors, especially the error of yaw angle, are large. After this magnetic orientation system was applied with our calibration methods and data fusion algorithm, the error of yaw angle was <3° and the attitude (pitch and roll) errors were <2°. At last, the precision comparisons between different data fusion algorithms are shown in Table 5. The above experimental results show that our magnetic

Table 4 Heading accuracies of different calibration methods in different attitudes

Different attitudes	Error separation, deg	Ellipsoid fitting, deg [5]	Traditional method, deg [7]
pitch = 0°, roll = 0°	0.2	0.4	0.8
pitch = −30°, roll = −30°	0.3	0.8	1
pitch = −60°, roll = 60°	0.4	1.2	1.6

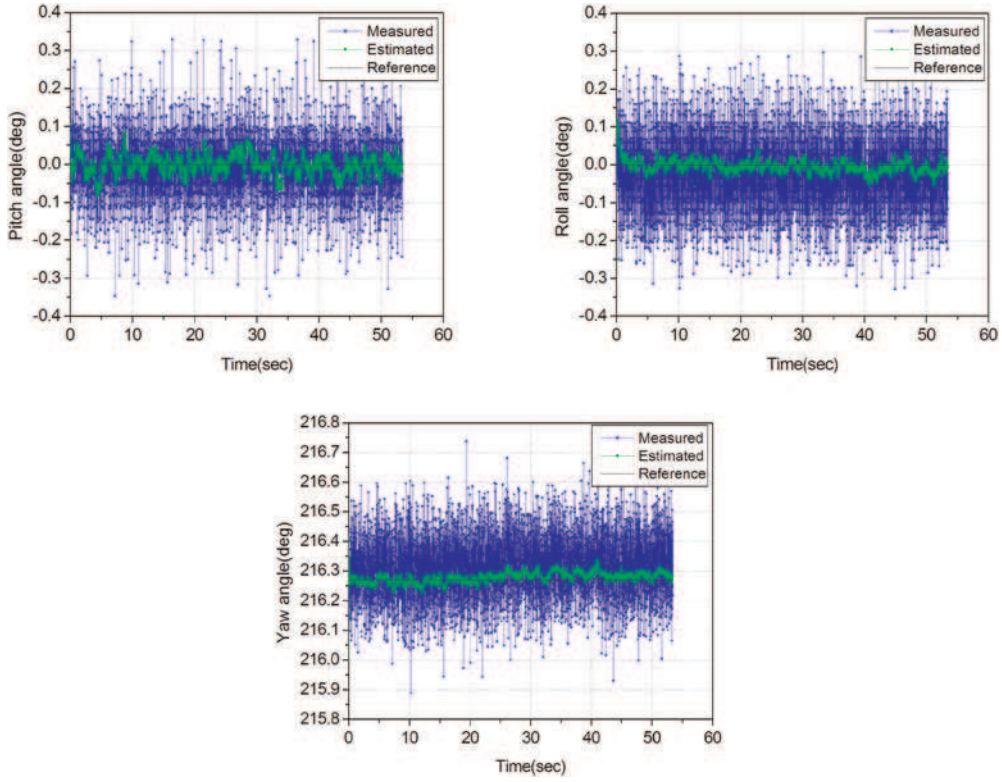

Fig. 3 *Test in Mode 1: Outputs of pitch, roll and yaw angles in a static state*

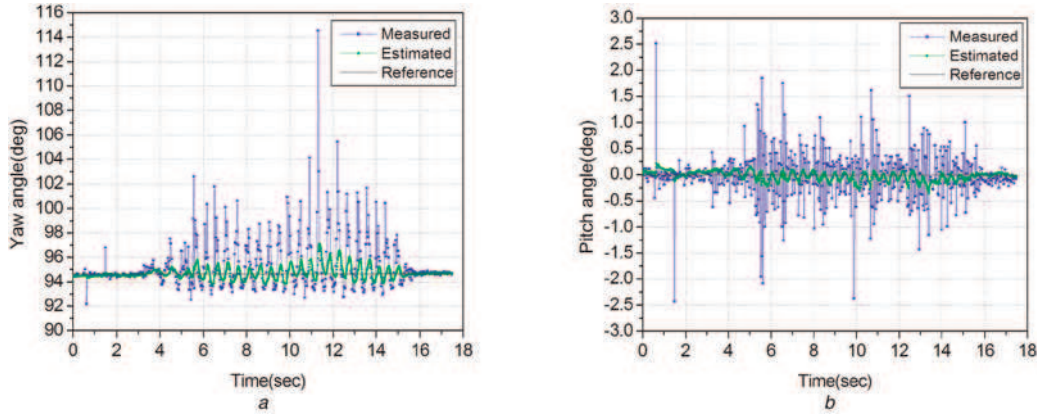

Fig. 4 *Test in Mode 2 (a): Outputs of yaw and pitch angles in the dynamic state when the roll angle was dynamically changed*

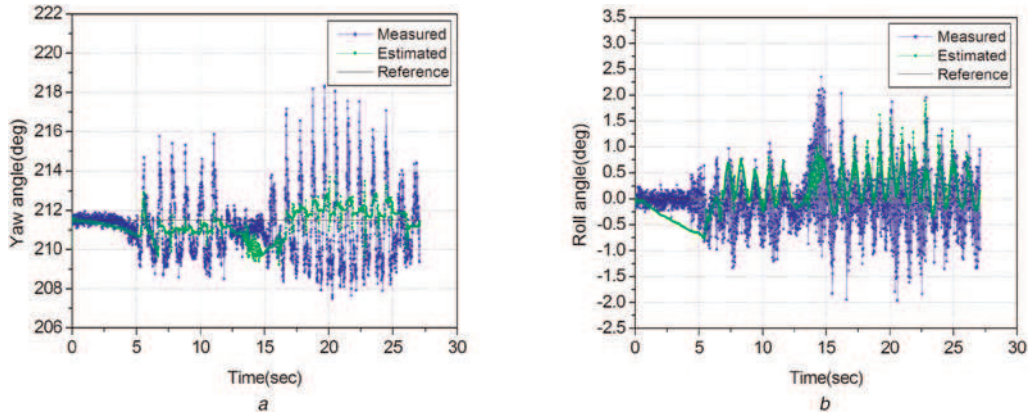

Fig. 5 *Test in Mode 2 (b): Outputs of yaw and roll angles in the dynamic state when the pitch angle was dynamically changed*

Table 5 Heading accuracies of different data fusion methods in static and dynamic state

Maximum error	Proposed KF (*q*-KF), deg	EKF, deg [9, 17]	CF, deg [13, 15, 16]
static	0.1	0.2	0.8
pitch dynamic	2.5	3.2	3.8
roll dynamic	2.8	3.6	3.9

orientation system has good performance and practicability even in dynamic work conditions.

6 Conclusions

In this paper, the magnetic orientation system was developed with three magnetometers, a tri-axis accelerometer and a tri-axis gyroscope. Magnetometer and accelerometer were calibrated with the error-separation method and six-position method, respectively. Moreover, the method of three-position with six different angular velocities was adopted for calibrating gyroscope. Finally, in order to keep the functionality of the magnetic orientation system in the dynamic state, a data fusion algorithm based on linear KF (*q*-KF) was developed. The experimental results show that the accuracy of the heading and attitude was improved significantly both in static and dynamic states after the improved data fusion. The maximum error of the yaw angle was about 0.1° in a static state and 2.8° in a dynamic state. Moreover, the maximum error of attitude (pitch/roll angle) was about 0.1° in a static state and 1.8° in a dynamic state. The achievement of magnetic orientation system with high precision demonstrated that the methods of calibration and the data fusion algorithm were effective and practical. It is worth mentioning that in terms of the estimation accuracy, due to the various dynamic conditions this paper does not claim that the parameters of KF are effective and suitable in any dynamic condition. In other words, the kinematic condition must be considered in terms of the severity of the external accelerations in order to improve the estimation performance by adjusting the parameters of KF. Thus, a future research direction will be focused on an adaptive algorithm for learning the parameters in real time to further improve the adaptability of magnetic orientation systems.

7 Acknowledgment

The research was supported by the National Natural Science Foundation of China (Project no.: U1732152).

8 References

[1] Ladetto, Q., Seeters, J.V., Sokolowski, S.S., *et al*.: 'Digital magnetic compass and gyroscope for dismounted soldier position & navigation'. Proc. NATO-RTO Meetings, Istanbul, Turkey, 2002

[2] Sipos, M., Rohac, J., Novacek, P.: 'Improvement of electronic compass accuracy based on magnetometer and accelerometer calibration', *Acta Phys. Pol. A*, 2012, **121**, (4), pp. 945–949

[3] Včelák, J., Ripka, P., Kubík, J., *et al*.: 'AMR navigation systems and methods of their calibration', *Sens. Actuators A*, 2005, **123–124**, pp. 122–128

[4] Renaudin, V., Afzal, M.H., Gérard, L.: 'Complete tri-axis magnetometer calibration in the magnetic domain', *J. Sens.*, 2010, **2010**, pp. 23–59

[5] Fang, J., Sun, H.H., Cao, J., *et al*.: 'A novel calibration method of magnetic compass based on ellipsoid fitting', *IEEE Trans. Instrum. Meas.*, 2011, **60**, (6), pp. 2053–2061

[6] Syed, Z.F., Aggarwal, P., Goodall, C., *et al*.: 'A new multi-position calibration method for MEMS inertial navigation systems', *Meas. Sci. Technol.*, 2007, **18**, pp. 1897–1907

[7] Yun, J., Ko, J., Lee, J., *et al*.: 'An inexpensive and accurate absolute position sensor for driving assistance', *IEEE Trans. Instrum. Meas.*, 2008, **57**, (4), pp. 864–873

[8] Chu, Z., Lin, X., Gao, K., *et al*.: 'Error-separation method for the calibration of magnetic compass', *Sens. Actuators A, Phys.*, 2016, **250**, pp. 195–201

[9] Sabatini, S.M.: 'Quaternion-based extended Kalman filter for determining orientation by inertial and magnetic sensing', *IEEE Trans. Biomed. Eng.*, 2006, **53**, (7), pp. 1346–1356

[10] Valenti, R.G., Dryanovski, I., Xiao, J.: 'A linear Kalman filter for MARG orientation estimation using the algebraic quaternion algorithm', *IEEE Trans. Instrum. Meas.*, 2016, **65**, (2), pp. 467–481

[11] Marins, J.L., Yun, X., Bachmann, E.R., *et al*.: 'An extended Kalman filter for quaternion-based orientation estimation using MARG sensors'. Proc. 2001 IEEE/RSJ Int. Conf. Intelligent Robots and Systems, Maui, USA, 2001, vol. 4, pp. 2003–2011

[12] Huang, Y.H., Rizal, Y., Ho, M.T.: 'Development of attitude and heading reference systems'. 2015 Int. Automatic Control Conf. (CACS), Yilan, Taiwan, 2015, pp. 13–18

[13] Gao, T., Shen, C., Gong, Z., *et al*.: 'An adaptive filter for a small attitude and heading reference system using low cost sensors'. Advances in Computer, Communication, Control and Automation, 2012, pp. 131–139

[14] Leccadito, M.T., Bakker, T., Niu, R., *et al*.: 'A Kalman filter based attitude heading reference system using a low cost inertial measurement unit', Virginia Commonwealth University, 2013

[15] Nowicki, M., Wietrzykowski, J., Skrzypczynski, P.: 'Simplicity or flexibility? Complementary filter vs. EKF for orientation estimation on mobile devices'. 2015 IEEE Second Int. Conf. Cybernetics (CYBCONF), Gdynia, Poland, 2015, pp. 166–171

[16] Naidoo, Y., Stopforth, R., Bright, G.: 'Quad-rotor unmanned aerial vehicle helicopter modelling & control', *Int. J. Adv. Robot. Syst.*, 2011, **8**, pp. 139–149

[17] Munguia, R., Grau, A.: 'Attitude and heading system based on EKF total state configuration'. IEEE Int. Symp. Industrial Electronics, Gdansk, Poland, 2011, pp. 2147–2152

[18] Peng, X.D., Chen, Y., Li, J.Y., *et al*.: 'Study on calibration method of MEMS 3-axis digital gyroscope', *Transducer Microsyst. Technol.*, 2013, **32**, (6), pp. 63–68

[19] Shuster, M.D.: 'Survey of attitude representations', *J. Astronaut. Sci.*, 1993, **41**, (4), pp. 439–517

[20] Lee, J.K., Park, E.J., Robinovitch, S.N.: 'Estimation of attitude and external acceleration using inertial sensor measurement during various dynamic conditions', *IEEE Trans. Instrum. Meas.*, 2012, **61**, (8), pp. 2262–2273